International Journal of Applied Earth Observations and Geoinformation 104 (2021) 102512

Contents lists available at ScienceDirect

International Journal of Applied Earth Observations and Geoinformation

journal homepage: www.elsevier.com/locate/jag

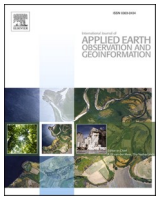

Novel low-cost mobile mapping systems for forest inventories as terrestrial laser scanning alternatives

Martin Mokroš [a,b,*], Tomáš Mikita [c], Arunima Singh [a], Julián Tomaštík [d], Juliána Chudá [d], Piotr Wężyk [e], Karel Kuželka [a], Peter Surový [a], Martin Klimánek [c], Karolina Zięba-Kulawik [e], Rogerio Bobrowski [e,f], Xinlian Liang [g,*]

[a] Faculty of Forestry and Wood Sciences, Czech University of Life Sciences Prague, Kamycká 129, 16500 Prague, Czech Republic
[b] Department of Forest Harvesting, Logistics and Ameliorations, Faculty of Forestry, Technical University in Zvolen, T. G. Masaryka 24, 960 01 Zvolen, Slovakia
[c] Department of Forest Management and Applied Geoinformatics, Faculty of Forestry and Wood Technology, Mendel University in Brno, Zemědělská 3, 61300 Brno, Czech Republic
[d] Department of Forest Resources Planning and Informatics, Faculty of Forestry, Technical University in Zvolen, T. G. Masaryka 24, 960 01 Zvolen, Slovakia
[e] Department of Forest Resource Management, Faculty of Forestry, University of Agriculture in Krakow, 31-425 Krakow, Poland
[f] Department of Forest Engineering, Midwestern State University, 84.505-677 Irati, Brazil
[g] The State Key Laboratory of Information Engineering in Surveying, Mapping and Remote Sensing, Wuhan University, 430070 Wuhan, China

ARTICLE INFO

Keywords:
Terrestrial laser scanning
Mobile laser scanning
Photogrammetry
LiDAR
Forest

ABSTRACT

The development of devices capable of generating three-dimensional (3D) point clouds of the forest is flourishing in recent years. It is possible to generate relatively dense and accurate 3D data not only by terrestrial laser scanning but also mobile laser scanning, personal laser scanning (hand-held or in a backpack), photogrammetry, or even using smart devices with Time-of-Flight sensors. Each of the mentioned devices has their limits of usability, and different method to capture and generate 3D point clouds needs to be applied. Therefore, the objective of our experiment was to compare the performance of low-cost technologies capable of generating point clouds and their accuracy of tree detection and diameter at breast height estimation. We tested a multi-camera prototype (MultiCam) for terrestrial mobile photogrammetry constructed by authors. This device is capable of capturing images from four cameras simultaneously and with exact synchronization during mobile data acquisition. Secondly, we have designed and conducted a data collection with iPad Pro 2020 using the new built-in LiDAR sensor. Then we have used mobile scanning approach applied a hand-held personal laser scanning (PLS_{hh}) using GeoSlam Horizon scanner. Moreover, we have used terrestrial laser scanning (TLS) using FARO Focus s70. With all mentioned devices, we have focused on individual tree detection and diameter at breast height measurements by cylinder-based algorithm across eight test sites with dimensions 25x25 m. Altogether, 301 trees were located on test sites, and 268 were considered for the analysis and comparisons (DBH $>$ 7 cm). TLS provided the most accurate and reliable data. Across all test sites, we achieved the highest accuracy (rRMSE ranged from 3.7% to 6.4%) and tree detection rate (90.6–100%). When we have considered only trees with DBH higher than 20 cm, the tree detection rate was 100% across all test sites (altogether 159 trees). When the threshold of trees considered in the evaluation was changed to 10 cm and then to 20 cm (from 7 cm), the accuracy (rRMSE) and tree detection rate increased for all devices significantly. Results achieved (DBH $>$ 7 cm) by iPad Pro were closest to TLS results. The rRMSE ranged across test sites from 8.6% to 12.9% and tree detection 64.5% to 87.5%. PLS_{hh} and MultiCam, the rRMSE ranged from 13.1% to 24.9% and 14% to 38.2%, respectively. The tree detection rate ranged from 55.6% to 75% and 57.1% to 71.9%, respectively. The time needed to conduct data collection on a test site was fastest using MultiCam (approx. 8 min) and slowest using TLS (approx. 40 min).

* Corresponding authors at: Faculty of Forestry and Wood Sciences, Czech University of Life Sciences Prague, Kamycká 129, 16500 Prague, Czech Republic (M. Mokroš).

E-mail addresses: mokros@fld.czu.cz (M. Mokroš), tomas.mikita@mendelu.cz (T. Mikita), singha@fld.czu.cz (A. Singh), tomastik@tuzvo.sk (J. Tomaštík), xchuda@is.tuzvo.sk (J. Chudá), p.wezyk@ur.krakow.pl (P. Wężyk), kuzelka@fld.czu.cz (K. Kuželka), surovy@fld.czu.cz (P. Surový), martin.klimanek@mendelu.cz (M. Klimánek), karolina.zieba@urk.edu.pl (K. Zięba-Kulawik), rogerio@unicentro.br (R. Bobrowski), xinlian.liang@whu.edu.cn (X. Liang).

https://doi.org/10.1016/j.jag.2021.102512
Received 10 June 2021; Received in revised form 10 August 2021; Accepted 19 August 2021
Available online 1 September 2021

1. Introduction

The development of new measurement techniques (e.g., laser scanning, or LIDAR) and the increasement of computational power of personal and mobile devices have in the last two decades changed the traditional inventory of forest properties and structures (Liang et al., 2016). New techniques provide new possibilities for users to take the forest to the laboratory and evaluate the needed characteristics in post-processing, e.g., in three-dimensional (3D) spaces. This procedure widens the possibilities to investigate forest conditions compared with traditional measures (tree height, diameter at breast height (DBH), trunk position).

3D data is useful in forest inventory and modelling applications, especially when combined with advanced visualisation techniques (Fabrika et al., 2018). However, the adoption of mentioned methods is limited by several constraints. Terrestrial laser scanners (TLS) are generally expensive and laborious in the field, although their spatial accuracy is very high (Liang et al., 2018a). The Structure-from-Motion (SfM) photogrammetry is easy to use from the user point of view, which relies on low-cost camera measurement equipment. The results are, however, highly dependent on the user's experience and the data-acquirement methodology that is complicated under conditions of unstructured environments, e.g. (Liang et al., 2015; Mokroš et al., 2018; Piermattei et al., 2019).

These limitations inspired efforts to bring the technologies able to produce 3D point clouds in a ready-to-use manner. One of the directions is the development and deployment of mobile laser scanners (MLS) (Čerňava et al., 2019; Forsman et al., 2016b; Kukko et al., 2012; Liang et al., 2014, 2018b) and hand-held personal laser scanners (PLS_{hh}) (Balenović et al., 2021). This approach overcomes the static nature of terrestrial laser scanning (TLS) and mitigates occlusion effects. MLS and PLS_{hh} use Simultaneous Localization and Mapping (SLAM) (Durrant-Whyte and Bailey, 2006) to merge trajectories. The SLAM determines the "pose" of the device (position and orientation in a local coordinate system) at a particular moment using recognized features and simultaneously generates a map of the surroundings. The method can be conducted in real-time, but the results can be often improved in post-processing.

The methods of MLS and PLS_{hh} eliminated some limitations of TLS. On the other hand, MLS and PLS_{hh} typically have lower spatial accuracy, and many studies reported mismatches between different trajectories (Čerňava et al., 2019; Liang et al., 2018b).

The next logical step to promote the wide use of 3D information in vast daily applications is to improve the sensor availability to average users. With this regard, the sensors using infrared light were adopted using two measurement principles: "structured light" and "time-of-flight (ToF)" (Sarbolandi et al., 2015), with the latter being more suitable also for outdoor measurements. Concepts of the 3D reconstruction using mentioned sensors were evaluated by Microsoft Kinect cameras (Hyyppä et al., 2018; McGlade et al., 2020; Wasenmüller and Stricker, 2017). In 2014, Google announced the "Project Tango", where the sensors were incorporated into mobile phones. The technology was based on three functionalities: depth perception (measuring of distances), motion tracking (using visual-inertial odometry) and area learning (recognition of already known features). The first two devices – a phone (codename Peanut) and a tablet (Yellowstone) were only available to developers. The first commercial device was the Lenovo Phab 2 Pro phablet, followed by the Asus Zenfone AR. The support for the technology was stopped in March 2018, most probably due to negligible success in the main area of interest – augmented and virtual reality. However, the 3D reconstruction capabilities were evaluated by researchers in many areas, including cultural heritage (Boboc et al., 2019; Schöps et al., 2015), environment monitoring (Chudý et al., 2018) and others. Despite the short lifespan, forestry applications were reported mainly aiming at diameters and positions of trees (Fan et al., 2018; Hyyppä et al., 2018; Tomaštík et al., 2017). Currently, modified versions of ToF sensors are included in smartphones and tablets. In 2020, Apple announced its latest iPad Pro and iPhone 12 Pro/Pro Max, which integrated such a sensor. Following these recent technical progresses, it can be foreseen that there will be more and more low-cost solutions coming into professional and consumer market in the near future. 3D information of the environment will be easier to be collected, but the applicability of such acquired 3D information is still unclear. In this study, we compared four solutions and their performance in the capturing 3D point clouds within a forest environment, i.e., a professional TLS, a state-of-the-art PLS_{hh}, a consumer-level mobile scanning using iPad Pro 2020 with a LiDAR sensor for the first time, and a self-developed multi-camera system for mobile photogrammetry (MultiCam). The idea of the multi-camera system is to provide a solution to compensate for the individual hand-held camera in order to achieve a successful mobile type of data acquisition. Among the four techniques, three sensors are based on active LiDAR sensors and one is based on passive sensors. All devices are compared with each other based on the tree detection rate, the accuracy of DBH measurements and the time needed for data acquisition.

2. Methodology

2.1. Test sites

The test sites are located in the middle of Slovakia within the Kremnica Mountains. Eight research plots with 25 × 25 m dimensions were established (Fig. 1).

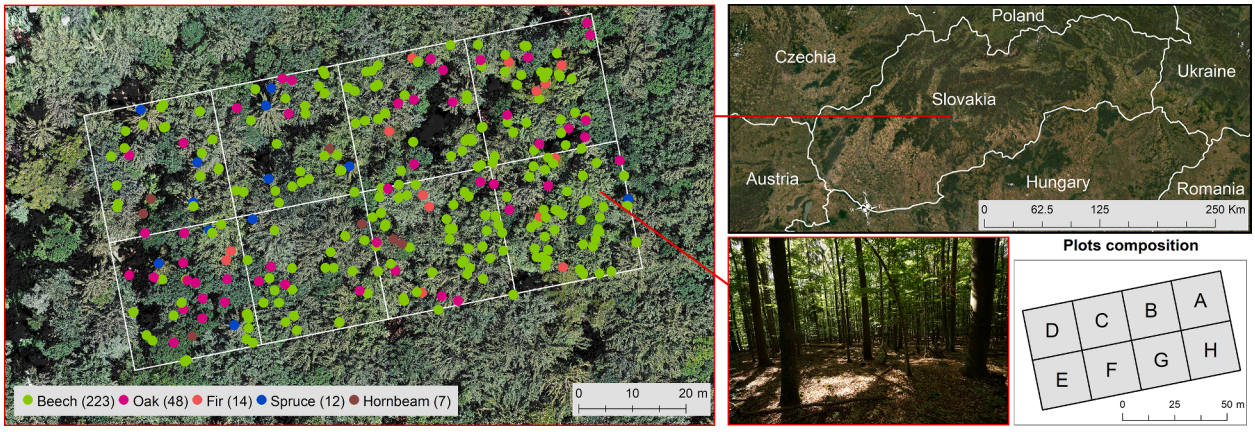

Fig. 1. The overview of all test sites with positions of individual trees (points – tree species based) and borders of research plots (white line) is on the left. On the top right is a position of plots within Slovakia. On the bottom right is a composition of test sites and a photograph from the research plot H.

Table 1
Range and mean of diameter at breast height across test sites with number of trees.

Plot	DBH range (cm)	DBH avg. (cm)	No. of trees	Density (trees/ha)
A	3.3–63.3	22.2	41	656
B	3.1–57.7	25.1	36	576
C	4.7–68.6	27.7	32	512
D	5.1–71.7	30.1	26	416
E	3.9–59.7	26.3	34	544
F	7.4–74.3	31.4	28	448
G	4.7–55.9	21.3	50	800
H	3.8–54.8	22.2	54	864

The number of trees varied from 26 to 54 across test sites (all trees considered) with dominant tree species European beech (*Fagus sylvatica* L.) and Norway spruce (*Picea abies* (L.) H. Karst.). In total, there are 301 trees and 268 trees have a diameter greater than 7 cm. The mean DBH varied from 21.3 cm to 31.4 cm across research plots (Table 1). The mean DBH of all trees was 25.0 cm.

2.2. Conventional in-situ measurements

Trees within each test site were measured by total station Topcon GPT3000M, and perimeters of trees were measured by measuring tape. Firstly, two orientation points and the first position of the total station, representing the first corner of the research plot were built up. The points were measured using the GNSS receiver Topcon Hiper SR combined with the total station Topcon 9000. The corners of the remaining research plots represent the corners of the grid with dimensions 25 × 25 m. They were calculated using coordinate increments of 25 m in the directions of the X and Y axes based on the first total station position, staked out by the total station, and permanently stabilised. The data set was collected with the aim to reach the highest allowed coordinate and elevation errors at the level of 0.02 m, using the corner points as a base for calculation of other consequential objects-representing points.

Afterwards, the position and perimeters of trees and the position of targets were measured for georeferencing purposes. All data were collected from one total station position in the middle of the plots, and two corner points were used as orientation points. The position for the machine was chosen so that all trees could be seen from one place (it was possible in most cases). The six targets oriented to the plot centre were evenly distributed in the plots, and their polar coordinates were measured in a non-prism operation mode. The polar coordinates of the trees at the height of 1.3 m were measured by length offset of the spatial polar method. According to the perimeter of trees, the lengths were adjusted by the radius of a particular individual during office processing. All polar coordinates were transferred to Cartesian coordinates after that.

2.3. Data acquisition and pre-processing

In the experiment, we used four devices: TLS, PLS_{hh}, Apple iPad Pro 2020 with LiDAR sensor (iPad), and a prototype of a multi-camera system (MultiCam). Two main distinguishing parameters are data acquisition approach, i.e., static (TLS) and mobile (PLS_{hh}, iPad, MultiCam), and the type of sensor used, i.e., active (TLS, PLS_{hh}, iPad) and passive (MultiCam).

We have approached data acquisition paths (Fig. 2) and pre-processing workflows differently based on the device properties and capabilities. However, for the same device, the workflow was the same across all research plots, and the processing to final tree positions and DBH estimation was also similar for all point clouds.

2.3.1. Terrestrial laser scanning

In the experiment, we used a Faro Focus s70 laser scanner (FARO Technologies, Inc., Florida, USA). It has a range from 0.5 to 70 m. The accuracy is ±2 mm on 10 m or ±3.5 mm on 25 m. We have used the resolution (point spacing) of 6.14 mm/10 m. One scan took 2 min and 24 s (2 kpt/sec). The advantages of the scanner, important for forestry use, are small dimensions (230 × 183 × 103 mm) and low weight (4.2 kg including battery). Since the scanner is a shift-based type of scanner, the scanning time is quite fast and at the same time with a high number of captured points.

A multi-scan approach was used to scan all research plots. Eight positions were placed on the border or near the border of the research plot and one in the centre of the research plot. The positions on the border were placed near the corners and near the middle of the plot side. The placement was based on the condition of each plot with regards to achieving the lowest occlusions (Fig. 2).

Plastic spheres were placed in the research plots for the purpose of the individual scan merging. Within each plot, twelve spheres were placed inside of the plot. With such a number of spheres and altogether nine scan positions, it was secured that more than four spheres were seen from each scanning position. Merging and georeferencing of the point clouds were done in Faro Scene software (ver. 2020.0.6) using the default workflow. We have used artificial black and white targets on tree trunks to georeference all merged point clouds to the System of the Unified Trigonometrical Cadastral Network (S-JTSK, EPSG:5514).

2.3.2. Hand-held personal laser scanning

The data acquisition by PLS_{hh} was performed using a GeoSLAM Horizon scanner (GeoSLAM Ltd., Nottingham, UK). It has a collection rate of 300,000 points per second, an accuracy of 1–3 cm and a range of 100 m. Before the scanning, it was necessary to place plastic spheres for

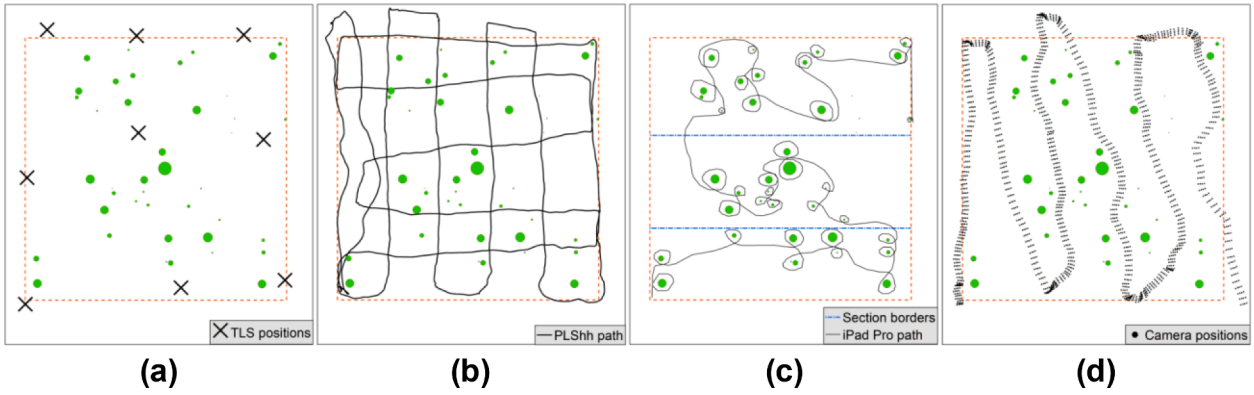

Fig. 2. Data acquisition positions (cross) and paths (black line) of all used devices on an example of plot A. Green circles represent tree positions, and their size is proportional to the diameter measured in the field. Paths of *a, b* and *d* are actual paths derived from devices. In the case of *c*, the path is illustration of the actual scanning path.

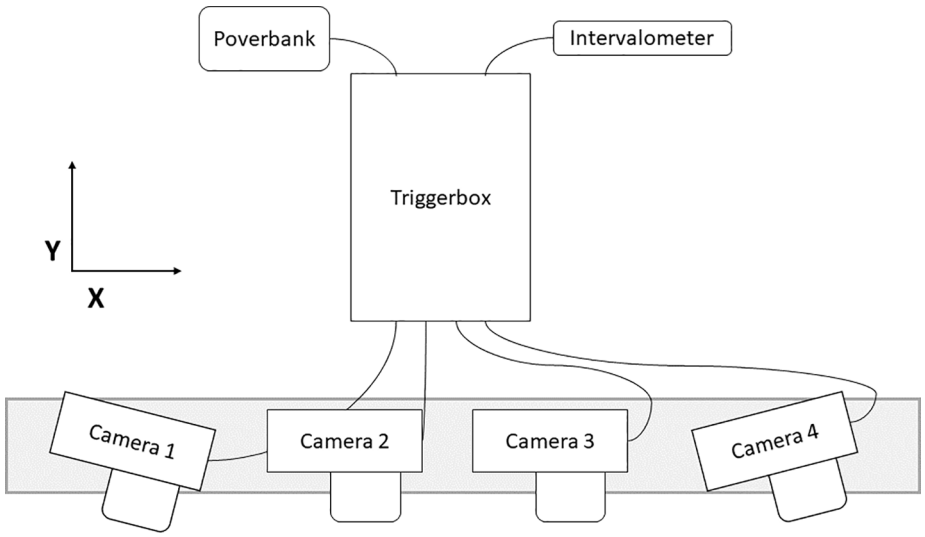

Fig. 3. The scheme of the multi-camera system. Cameras are connected directly to Triggerbox, which is powered by a powerbank and controlled by an intervalometer. Below are examples of images from each camera from plot A from the same position during the mobile imagery.

the subsequent georeferencing of the point cloud. It was not possible to use markers placed on trunks since they were not adequately visible due to the noise. The spheres were placed at the four corners of each plot and scanning always started in the upper right corner and proceeded along the lines at about 5 m intervals with a subsequent cross pass with a diagonal return to the starting point (Fig. 2b). This measurement method was chosen in order to obtain a higher density of points. The data acquisition in one plot, including the placement of reference spheres, did not exceed 10 min.

GeoSLAM Hub software (ver. 5.3.1) was used for post-processing of scanned data, and subsequently, point clouds from each surface were georeferenced into the JTSK system in GeoSLAM Draw software (ver. 3.1). During processing in GeoSLAM HUb, we used default parameters and workflow.

2.3.3. *iPad pro scanning*

The third device used for scanning the study sites was a 4th generation iPad Pro 2020 tablet (Apple Inc. San Francisco, USA). This is the generation that is equipped with an Apple LiDAR sensor able to scan the environment. Based on the information that Apple has not officially announced, the sensor is a direct time-of-flight custom-designed LiDAR scanner that also uses a camera and motion sensor to measure depth. The sensor is able to scan up to 5 m. We have used a 3d Scanner App (Laan Labs, New York, USA). The app also provides the possibility to colourise and export mesh and point clouds.

Since the range of the scanner is 5 m, we have used a different approach of data acquisition as with other mobile devices (PLS_{hh}, MultiCam). The plots were divided into three segments, and the path started in the first segment, and the operator walked around each tree in sequence. And when all trees were scanned, the path continued to the following segment (Fig. 2c). In the iPad measurement, the operator needed to carefully walk around trees and avoid rescanning already scanned trees. In cases where rescanning of already scanned trees was done, the reconstruction of such trees got worse. In some cases where trees were very near each other, it was necessary to scan them together.

During pre-processing of point clouds, we have found out that it was

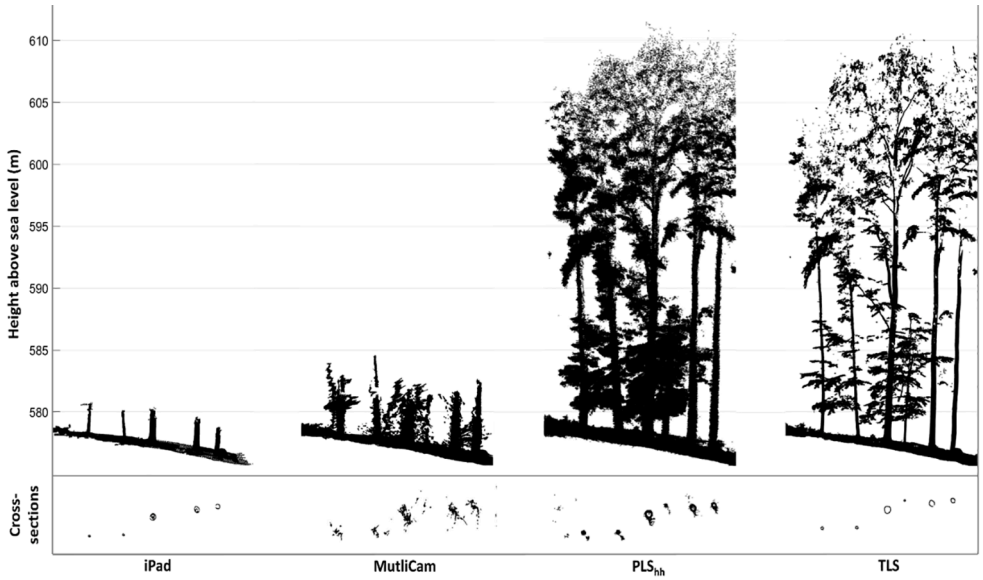

Fig. 4. Examples of point clouds from all devices in Plot B in the side view (top) and 5 cm cross-section at DBH height (below), i.e., 1.275–1.325 cm above the ground.

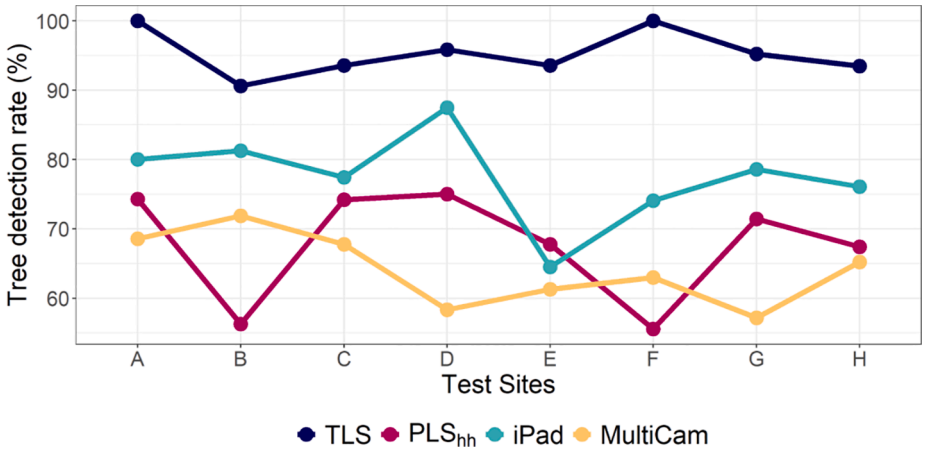

Fig. 5. Tree detection rate of all devices used across eights plots.

not possible to use markers that were placed on tree trunks for georeferencing. Due to this fact, resulting point clouds were aligned with point clouds from TLS in CloudCompare using Iterative Closest Point (ICP) algorithm. It was necessary to georeference point clouds to be able to compare them with reference data.

2.3.4. *Multi-camera mobile photogrammetry*

Data acquisition by mobile photogrammetry was done by the multi-camera prototype (MultiCam) constructed by authors. The MultiCam consists of four cameras placed on the aluminium profile. We have used Sony a6300 cameras with Sony 10–18 mm F4 OSS lens (Sony Corp., Tokyo, Japan). Two middle cameras were facing in the walking direction, and two cameras on edge have been shifted to the side (Fig. 3). The overlap of at least 60% on 3 m was ensured between edge and middle camera pairs. The overlap was checked before each plot imagery.

We have controlled the imagery capturing by TriggerBox (Esper Ltd., Nottingham, United Kingdom). This device is a multi-camera shutter controller which can control up to six cameras at once. The synchronisation of the shutter for all cameras is secured by very low delay (0.000002 s). The TriggerBox was powered by a powerbank (5,000 mAH), and the shutter was controlled by an intervalometer.

The whole MultiCam system weighs 4.1 kg. It consists of four cameras with lenses (2.5 kg), rig (0.9 kg), TriggerBox with cables (0.45 kg), intervalometer (0.12 kg) and powerbank (0.1 kg). The price is approximately 7,200 euros, where 6,800 euros is for cameras with lenses.

The image capturing was set to one image per second for each camera simultaneously. The path of data acquisition consists of six strips. The distance between strips was approximately 5 m. The MultiCam was facing in the walking direction. On turns, the walking speed was slowed down to ensure high overlap. The number of images ranged through plots from 1,616 to 1,916 (median = 1,850) with all four cameras considered. The number of positions per plot ranged from 404 to 479 (median = 462.5).

The camera settings were adjusted accordingly to the light conditions. Since the mobile approach for data acquisition was used in this experiment, the shutter speed was set to 1/320 s. The ISO was set to 3200 and aperture to 7.1.

Processing of images to georeferenced point clouds was done using Agisoft Metashape (Agisoft LLC, Saint Petersburg, Russia). Firstly, we calibrated the camera using a chessboard screen and the calibration module within the Agisoft Metashape. We have captured images from multiple angles following the calibration protocol from Agisoft documentation. The calibration file was then used within the alignment

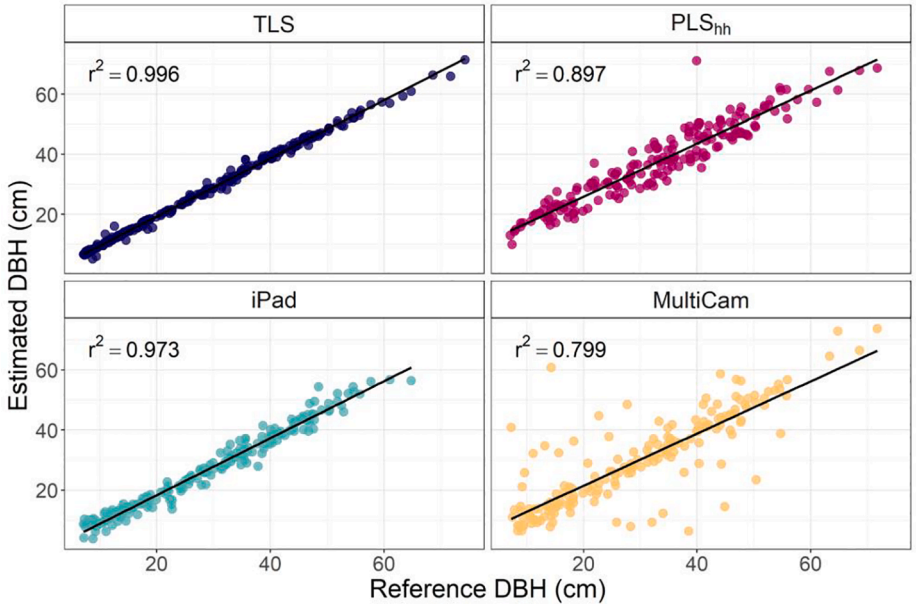

Fig. 6. Conventional and point cloud based methods for DBH measurement, according to each device used, with its regression line and r squared.

Table 2
Results of tree attribute estimation (when all trees across eight plots were considered), i.e., root mean square error and bias in both absolute and relative values, tree detection rate (TDR), false tree detection (FTD) for devices used across all eight plots. Then we report data acquisition time per plot, the weight of the devices with all necessary accessories and approximate price (sources: echosurveying.com and amazon.com).

	RMSE (cm)	rRMSE (%)	Bias (cm)	rBias (%)	TDR (%)	FTD (No.)	Time (min)	Weight (kg)	Approximate Price $
TLS	1.45	5.18	−0.98	3.48	95.15	12	40	6.2	20,970
PLS_{hh}	6.26	18.88	4.34	13.11	67.91	10	10	3.8	30,350
iPad	3.14	10.89	−2.12	7.35	77.24	0	15	0.5	799
MultiCam	6.98	22.86	−0.78	2.56	64.18	137	8	4.1	7,200

process. The images were aligned with "High quality", which is the original resolution of images. We have not used any preselection, which means each image was compared to each image in the dataset. After alignment, we manually searched for markers that were placed on trunks. Markers were used to georeference the tie point cloud to S-JTSK system. On each plot, at least four markers were found. Next step, the densification of tie points was performed with medium quality. Generated point clouds were exported for tree detection and DBH estimation.

The examples of point clouds with their cross-sections at 1.3 m are shown in Fig. 4. Differences in the point-cloud data quality can be clearly seen from the cross-section sub-figures, where the TLS data has the highest level of data accuracy, iPad also provide data with little noise, and MultiCam and PLS_{hh} contain clear noise.

2.4. Tree detection and DBH estimation

The point cloud data from stationary TLS and mobile PLS_{hh}, iPad and MultiCam were processed through the same processing chain as described in (Liang et al., 2018b).

The TLS, PLS_{hh} and MultiCam point clouds were sampled. The point closest to the centre of gravity within each 1 cm voxel was selected. The sampling process gives a comparable data set of the original point cloud in the sense of the point distribution, where the gravity is a unique point that the position vectors relative to this point sum to zero and the point closest to the gravity faithfully represents this unique point without introducing any additional measurement errors. The original point clouds from the iPad were used because of its low resolution.

The DTM was reconstructed using a morphological filter and linear interpolation. Stem points were identified through point-based analyses. Point distributions were studied within their immediate neighbourhood, where potential stem points have vertical planar structures. Tree stem models were built from the recognised stem points as a series of 3D cylinders representing the stem growth. The DBH and location of a stem were estimated from the cylinder element at the breast height (1.3 m above the ground).

2.5. Data evaluation

The tree positions and diameter estimation have been calculated for point clouds generated by each device for all eight plots. These estimated trees were matched with field data measured by total station and measuring tape. For each reference tree, a buffer with a 1 m radius was made to help to locate matches. The pairing was done manually in ArcGIS for desktop 10.7 (ESRI, California, USA) to ensure the correctness of matches.

When all pairs were identified, we calculated estimation errors. Errors were calculated by subtracting reference diameter with estimated diameter (1). To exclude gross error, we have deleted estimated DBH when the relative DBH error exceeded 100% of that particular tree (2).

$$DBH_{err} = DBH_{es} - DBH_{r}. \quad (1)$$

$$rDBH_{err} = (DBH_{es}\tilde{A}\cdot DBH_{err})*100. \quad (2)$$

where DBH_{err} is a calculated error of estimated DBH, DBH_{es} is a DBH estimated from point cloud, DBH_r is measured DBH in the field and $rDBH_{err}$ is relative error of estimated DBH.

Furthermore, bias, relative bias (rBias), root mean square error (RMSE), and relative RMSE (rRMSE) were calculated to compare the results between devices.

The tree detection rate was calculated based on correct matches between reference and estimated DBH. Falsely detected trees were also identified and reported.

One sample t-Test was used to statistically identify the significance of over- or underestimation of DBH by estimation. We have tested calculated errors of DBH estimation against zero.

A two-way analysis of variance (ANOVA) was used to identify the influence of the device and plot on the DBH estimation accuracy.

3. Results

3.1. Tree detection

The sum of trees with DBH higher than 7 cm is 268 across all test sites. The tree detection rate of all trees was as follows: 95.15% (TLS), 67.91% (PLS_{hh}), 77.24% (iPad), 64.18% (MultiCam).

TLS provided the highest tree detection rate overall. Within each plot, the detection rate ranged from 93.5% to 100%, where 100% tree detection rate was achieved on two plots. PLS_{hh} tree detection rate ranged from 55.6% to 74.3%, for iPad, it ranged from 64.5% to 87.5%, and for MultiCam, it ranged from 57.1% to 71.9% (Fig. 5, Table A1).

The highest amount of falsely detected trees was from MultiCam point clouds, through which 137 trees were falsely detected from an amount of 327 detected trees. The opposite was achieved by the iPad, where 0 trees were falsely detected across all plots. Then TLS had 12 and PLS_{hh} 10 falsely detected trees across all plots. The number of falsely detected trees for each plot and device is shown in the Table A2.

3.2. DBH estimation

The correlation between the reference and estimated DBH was highest when point cloud from TLS was used ($r^2 = 0.996$) and lowest for MultiCam ($r^2 = 0.799$) (Fig. 6). DBH estimated from iPad had also reached a high correlation similar to TLS ($r^2 = 0.973$).

The bias and relative bias for all considered trees measured from a point cloud of TLS, PLS_{hh}, iPad and MultiCam was −0.98 cm (3.48%), 4.34 cm (13.11%), −2.12 cm (7.35%) and −0.78 cm (2.56%) respectively (Table 2). The range across plots was −1.43 cm to −0.7 cm, 2.58 cm to 6.00 cm, −2.59 cm to −1.79 and −5.04 cm to 2.53 cm respectively (Tables A3 and A4).

The DBH estimated from TLS, iPad and MultiCam underestimated the conventional DBH measurements. For TLS and iPad, the underestimation was statistically significant. In the case of $PLS_{hh,}$ the DBH is significantly overestimated (Fig. 7). The significance of over- and underestimation was tested by One-Sample t-Test.

When all trees from eight plots were used to calculate RMSE and rRMSE, the highest accuracy was achieved by TLS with RMSE 1.45 cm and rRSME 5.18%. The least accurate results were achieved by MultiCam, where RMSE was 6.98 cm, and rRMSE was 22.86% (Table 2). When results are grouped by plots, TLS achieved the most accurate results across all plots with RMSE ranging from 1 cm to 2 cm and rRMSE

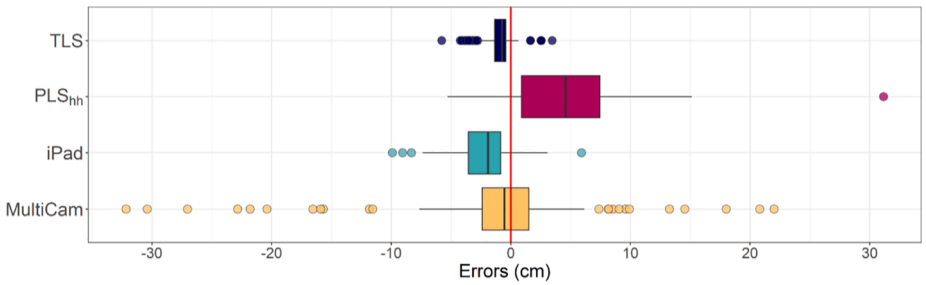

Fig. 7. Boxplots of absolute errors (cm), where boxplots correspond to the 25th and 75th percentiles and whiskers are 1.5 * interquartile range. The line inside the boxplots corresponds to the median. Dots represent outliers.

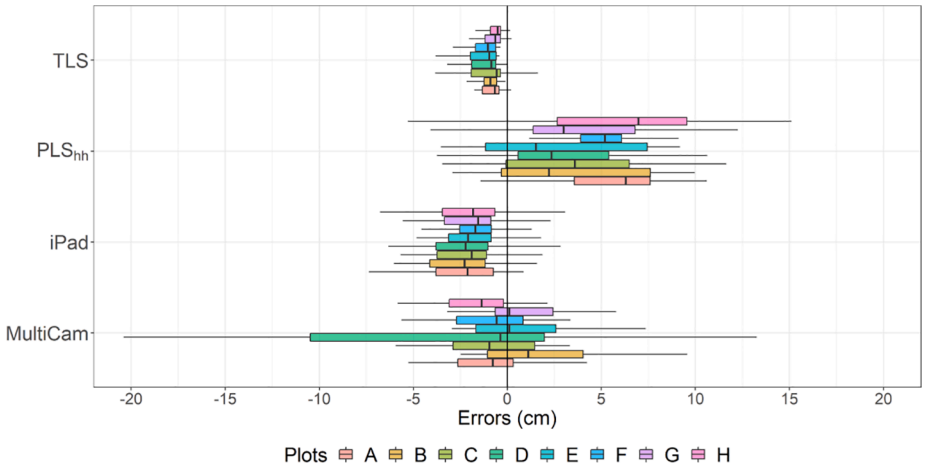

Fig. 8. Boxplots of absolute errors (cm). boxplots correspond to the 25th and 75th percentiles and whiskers are 1.5 * interquartile range. The line inside the boxplots corresponds to the median.

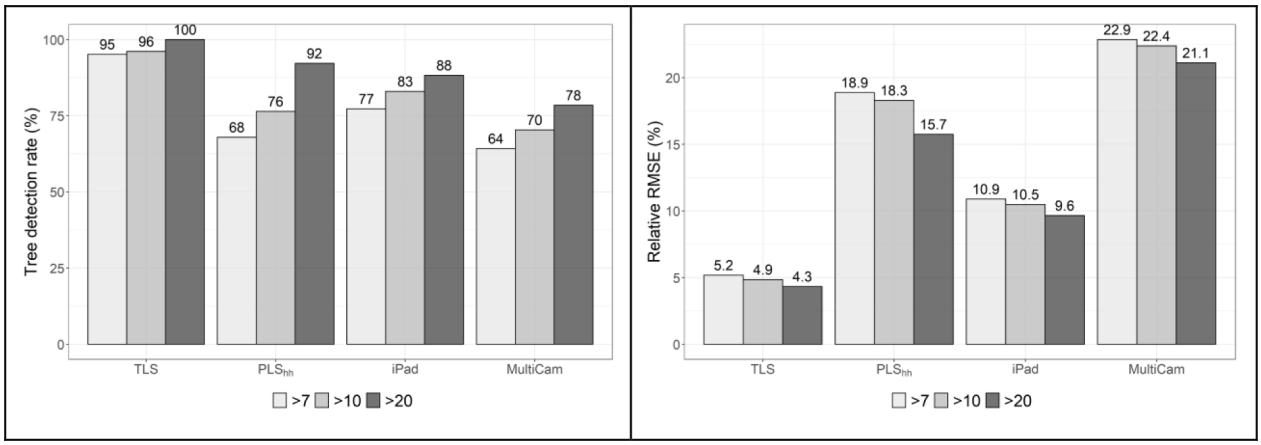

Fig. 9. The changes of tree detection rate (left) and rRMSE (right) for three DBH thresholds (7 cm, 10 cm and 20 cm) grouped by used devices.

from 3.7% to 6.4%. Regarding the least accurate results, the MultiCam has achieved it on six plots and PLS_{hh} on two plots (B and G). The range was 5.3 cm to 14.3 cm (18.8–38.2%) and 4.8 cm to 8.8 cm (13.1–24.9%), respectively. The iPad achieved RMSE 3.14 cm and rRMSE 10.89% when all trees were considered. The RMSE and rRMSE for all used devices for each plot are shown in Tables A5 and A6.

Two-way ANOVA was used to test the significant influence of devices, plots and their interaction on the accuracy of DBH estimation. The ANOVA indicates a significant impact of devices, plots and their interactions (Table A7). We have used the Tukey post hoc test to identify which devices, plots and interactions are significantly different from each other. When only devices were compared, only the difference between TLS and MultiCam was not statistically significant. When plots were compared, only the difference between Plot D and B was statistically significant. To compare interactions 496 pairs were made of those 154 were statistically significantly different from each other and 145 of them were pairs that contained PLS_{hh}. This difference can be clearly seen in Fig. 8. The remaining pairs that were significantly different were pairs of MultiCam plot B with all iPad plots.

3.3. DBH thresholds

Next, we have evaluated trees with DBH higher than 10 cm and 20 cm. The hypothesis is that the results for such trees are going to be more

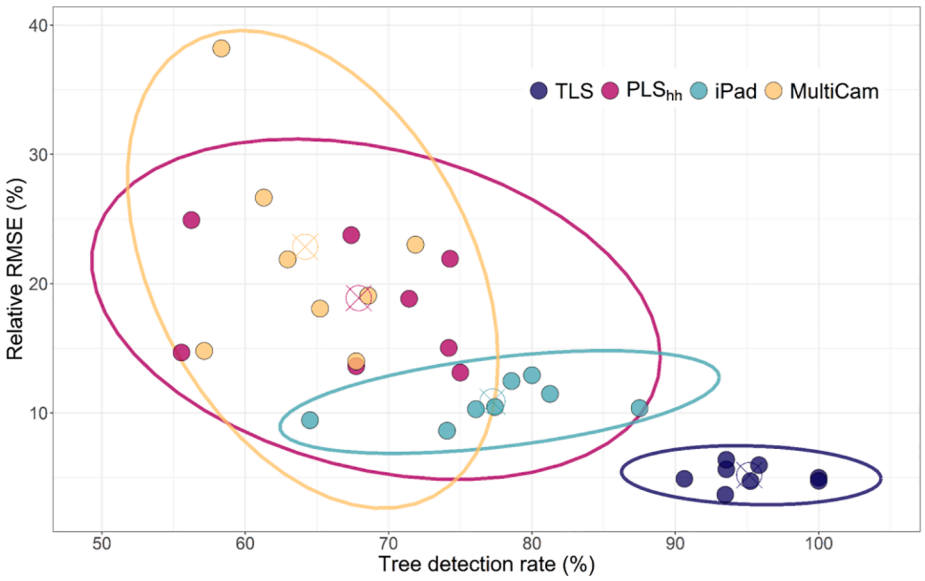

Fig. 10. Scatter plot visualising tree detection rate and rRMSE grouped by used devices. Each device has eight filled points (representing test sites) with one data ellipse and one crossed circle which represents an overall tree detection rate and rRMSE of trees with DBH larger than 7 cm.

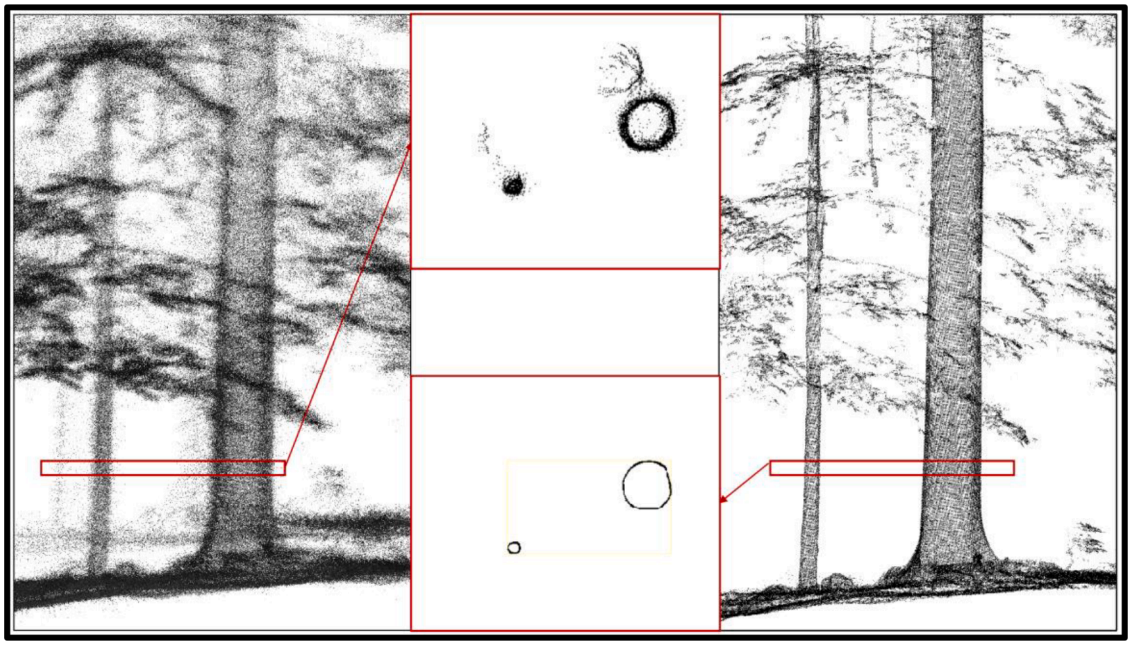

Fig. 11. The point clouds of two individual trees from PLS_{hh} (left) and TLS (right). A top view of 10 cm cross-sections at the breast height in both datasets is also illustrated in the middle.

accurate with a higher tree detection rate and the larger the tree size, the higher possibility is the correct detection/modelling. Across the plots, 301 trees were measured by conventional methods with all DBH sizes considered, 268 trees (89%) with DBH higher than 7 cm, 229 (76%) with >10 cm and 153 (51%) with >20 cm. The accuracy (rRMSE) and tree detection rate increased significantly and linearly for all devices when the threshold of DBH was changed to 10 cm and then to 20 cm (Fig. 9, Table A8).

4. Discussion

4.1. The overall evaluation on the extracted tree parameters

Results showed that DBH estimation from TLS point clouds is achieving the most accurate results together with the highest tree detection rate across all test sites and overall when compared to the other three mobile devices (Fig. 10). The reliable accuracy achieved by iPad Pro across all sites is showing a high potential for future applications, especially when other high-quality sensors and options of smart devices will be used. On the other hand, PLS_{hh} and MultiCam data have issues such as a high amount of noise and inaccurate alignments, results typically have lower accuracy.

The most visible advantage of TLS and PLS_{hh} is the long-range of the sensors. It is usually tens of meters and with scanners that we have used it was 70 m for TLS and 100 m for PLS_{hh}. Such range is sufficient for tree height measurements (Jurjević et al., 2020; Wang et al., 2019) or crown reconstruction. This is not feasible with iPad or MultiCam. The range of the iPad is 5 m. The MultiCam system is based on passive sensor

(camera). The range is based on the field of view of the camera and only objects captured at least from two positions are going to be reconstructed. Furthermore, the far objects are going to be reconstructed with lower detail than those close to the camera, since the ground sample distance (GSD) will be bigger. The example of point clouds from all devices of plot A are shown in Video 1.

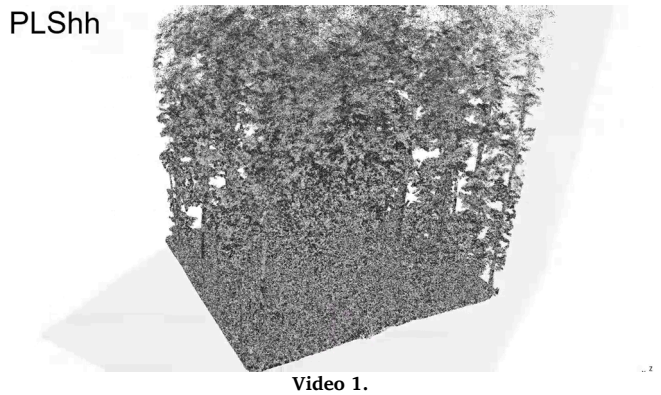

Video 1.

4.2. Hand-held personal laser scanning

Among published studies, the range of tree detection rate was 57–100% (Balenović et al., 2021). The highest rate (100%) tree detection rate for trees over 10 cm of DBH was reported by (Bauwens et al., 2016) over ten plots (331 trees) with different conditions. (Chen et al., 2019) achieved 90.9% tree detection rate for trees over 5 cm and with the same threshold (>5cm), authors (Gollob et al., 2020) achieved a tree detection rate higher than 95% within the majority of 20 plots. On the other hand, some authors achieved worse results. For example (Del Perugia et al., 2019) used three different data collection approaches, and with the one where the distance between strips was 15 m, the tree detection rate was 57%, but when the distance was decreased to 10 m, the tree detection rate was significantly higher (94%).

Based on these results, we assumed that the point cloud would be denser and the issue of occlusion would be significantly decreased if we would have use the distance between lines approximately 5 m and we would have also add perpendicular line paths. But our results rejected this hypothesis. The tree detection rate ranged from 56% to 75%. We assume that this approach brought a higher amount of data to be processed and aligned, which caused more geometric discrepancies. Within all plots, the trunks are not aligned precisely, and many trunks are misaligned themselves (Fig. 11). The problem of the forest environment is that there is an only small number of objects with clearly defined edges that could improve the alignment of the applied SLAM algorithm in the GeoSLAM. According to our results, the chosen trajectory with cross repetition tended to worsen rather than improve the SLAM results.

Although the PLS_{hh} method is promising in forestry, finding the optimal trajectory for data collection will require considerable effort. It is not possible to determine a single procedure for all forest types. Young forest stands with smaller DBH, and higher density will require different data collection than older stands with higher DBH.

When TLS was compared with PLS_{hh}, (Gollob et al., 2020) achieved higher tree detection by PLS_{hh}. This can be caused by the relatively low number of TLS scan positions (four with one in the centre). A similar comparison was done by (Ryding et al., 2015) where 54 trees were detected by TLS and 45 by PLS_{hh}. (Cabo et al., 2018) reported 100% agreement between TLS and PLS_{hh}, where both devices detected 271 trees across two plots.

Based on the review paper of (Balenović et al., 2021), the rRMSE of DBH estimation using PLS_{hh} varied from 3.5% (Hyyppä et al., 2020) to 23% (Ryding et al., 2015). The accuracy of DBH estimation achieved by us was from 13% to 25% and 18.9% overall. The accuracy increased significantly when the threshold of consideration was changed to 10 cm and 20 cm as an opposite of 7 cm. Overall it was changed to 18.3% and 15.7%, respectively. (Ryding et al., 2015) achieved 23% rRMSE when all trees were considered and 9% when only trees with DBH higher than 10 cm were considered. Furthermore, they also calculate rRMSE for trees smaller than 10 cm DBH and the rRMSE was 46%.

Our results also confirm the significant influence of DBH threshold of considered trees. The tree detection rate and accuracy of DBH estimation increased significantly when we have considered trees with DBH > 10 cm and then only those with >20 cm. This is clearly raising the important issue of where the threshold should be and how it will influence whole forest stand results.

4.3. Smart devices with ToF

The advantages of using smart devices such as smartphones or tablets is the easy manipulation (weight and size) and also familiarity with such devices within a majority of the population. Furthermore, in future, when additional sensors or functions of such devices are going to be explored and used for forestry applications, the employment will be even more reasonable. For example, the usage of GNSS data from smartphones for positioning within forest environment (Tomaštík et al., 2017). In recent years studies focused mainly on two paths. Firstly, the "Project Tango" where developers mainly focused on augmented reality applications. To be able to scan the environment, devices with infrared depth sensors were needed. For example, Lenovo Phab 2 Pro phablet. Authors (Fan et al., 2018; Hyyppä et al., 2018; Tomaštík et al., 2017) explored the application for the tree parameters estimation. The accuracy (rRMSE) achieved for DBH estimation within plots varied from 6.8% to 8.8% (Tomaštík et al., 2017) and from 2% to 11.1% (Fan et al., 2018). The results achieved within the presented study ranged from 8.6% to 12.6%. These results are similar and slightly worse than the previous reported studies. However, the main difference between the iPad Pro scanning and Google Tango approach is that Google Tango has implemented the SLAM algorithm with the "loop closure" detection, which improves the trajectory accuracy using the alignment of multiple-times scanned features. This algorithm is helping to localise the device without using a GNSS device or sensor.

The disadvantage when we have used the iPad to scan the plots was the removal of already scanned areas due to the lack of SLAM-like algorithm. We needed to always check whether we are far enough from already scanned trees to avoid rescanning them from faraway positions, which would lead to worse accuracy of such trees. Since the range is 5 m it was possible to avoid it in the majority of cases. But for more dense plots this can cause issues during scanning and will lead to worse accuracy. We believe that the implementation of the SLAM algorithm will help to eliminate such issues.

Besides Google Tango, Microsoft Kinect is another similar alternative. (McGlade et al., 2020) has conducted an experiment within an urban park with larger trees (mean DBH 73.4 cm). The data acquisition focused on individual trees, and it was static from a tripod with a different distance from the trunk (1–3 m). The RMSE ranged from 6.8 cm to 16.9 cm. What is approximately 9.2–23.0% of rRMSE (the average DBH was 73.4 cm).

4.4. Multi-camera photogrammetry

Few studies have been published which used more than one camera at once to conduct a photogrammetry image collection of forest stands. Moreover, we believe only (Forsman et al., 2016a) has dealt with more than two cameras at once. They used a camera rig with five cameras. Since the two cameras have been found to have insufficient optical stabilisation they were used just partially. Altogether 25 research plots with a 20 m radius were used. On these plots, images from the centre were taken from 12 positions. It was possible to sufficiently reconstruct point clouds on six plots for the DBH estimation and evaluation. The relative root mean square error varied from 12.4% to 60.5% within six

plots. The range of the presented study using MultiCam is 14.8–38.2%. The study of (Forsman et al., 2016a) used a multi-camera rig, but the data acquisition was static and only from the centre of a plot by three cameras and partially with two other cameras.

In our experiment, we have used mobile photogrammetry. In the majority of published papers on the subject of using terrestrial photogrammetry for measuring DBH is a static approach prefered or the so-called stop-and-go method. With this approach, the operator is taking images only when it is not moving with the camera on a tripod or in hand. When mobile is compared to a stop-and-go (static) approach, the advantage is faster data acquisition. In Mokroš et al. (2018), the average time needed to conduct mobile photogrammetry was slightly above 13 min, and by the stop-and-go method, it was 31 min on average for the same plot (35 × 35 m).

On the other hand, the mobile photogrammetry is more prone to fail to align images and generate sufficient and accurate point clouds. The operator is continuously moving and taking images. It is essential to secure a sufficient overlap between images. From our experience, the trickiest part of such data acquisition is the turning points outside the plot where the operator needs to turn back to the plot and do another line strip. In these places, the alignment photogrammetry process is failing most. Our hypothesis was that using multiple cameras in a row will greatly help to keep the overlap during the walking but also on those turning points. This hypothesis seems correct. We have aligned all images on turning points or in other parts of imagery paths. We have not needed to repeat data acquisition.

The challenge of mobile photogrammetry is the camera settings. Since the operator is constantly moving during imagery, the shutter speed must be quite high to avoid blurry images. When the shutter speed is high in a fairly dark environment, as the dense forest during vegetation season is, the ISO and aperture must be set appropriately to achieve bright enough images. In our case, we have used 1/320 s shutter speed, 3200 ISO and 7.1 aperture. The ideal combination for such data acquisition should be explored. If we change the shutter speed to faster values, the ISO and aperture should be adjusted, but we do not have an answer yet which settings will bring results with less noise and with higher accuracy. Regarding the stop-and-go method, the shutter speed can be slower especially when a tripod is used. This is the main advantage of the static approach versus the mobile one.

Overall terrestrial photogrammetry can provide high accuracy of DBH measurements. The RMSE can achieve sub-centimetre accuracy. Especially in cases where a stop-and-go approach is used and only one tree at a time is photographed. In Mokroš et al. (2020), authors used such an approach, and the rRMSE has not exceeded 1% in all 40 trees, and they were able to measure the annual trunk increment of mature trees. When authors focus on multiple trees at plots using a single camera, the rRMSE can vary from 2% (Mikita et al., 2016) to 61% (Forsman et al., 2016a). Results are highly dependent on the data acquisition approach, camera and lens, camera settings, forest stand parameters and so on.

In the present study, we have achieved an rRMSE range 14–38%. We believe that the results could be improved. In future experiments, we will focus on the different setup of cameras on the rig, higher number of cameras, composition, or orientation. Furthermore, the influence of different camera settings should be tested.

5. Conclusion

We presented here a comparison of well-known terrestrial laser scanning (TLS), state-of-the-art hand-held personal laser scanning (PLS_{hh}), laser scanning based on iPad Pro (hand-held) and mobile photogrammetry with a self-constructed multi-camera system (MultiCam). The comparison was based on the performance within forest stands focusing on tree detection, DBH estimation and overall performance. Altogether, eight plots (25 × 25 m), with 301 trees (602 trees per ha), were established. Data acquisition of one plot lasted 40 min (TLS), 10 min (PLS_{hh}), 15 min (iPad) and 8 min (MultiCam). TLS achieved tree detection above 90% for all eight plots. None of the other used devices reached a 90% tree detection rate. The highest range among them was when iPad was used 64.5% 87.5%. The tree detection rate range of PLS_{hh} and MultiCam was 55.6–74.3% and 57.1–71.9%, respectively. Similar results were achieved when the accuracy of DBH estimation was compared. TLS had RMSE under 2 cm for all plots. None of the other used devices reached such accuracy. Nevertheless, iPad performed the closest results, 2.6–3.4 cm.

Each device provides certain benefits. The advantage of TLS and PLS_{hh} is the coverage of the upper parts of trees. Therefore, also tree height or crown parameters are possible to measure directly from point clouds. On the other hand, both devices are significantly more expensive than the iPad or MultiCam. Thus, if the goal is to measure DBH, these devices could be the suitable alternative. However, further experiments have to be done within forests with different levels of complexity. Furthermore, experiments focusing on achieving 100% tree detection rate on the plot, and in the case of MultiCam, the focus should be on decreasing point cloud noise. Only iPad Pro is a solution that provides point cloud right away in the field. This advantage is highly usable for forestry practice, where operators can have results right away in the field. On the other hand, the data acquisition must be done very carefully to avoid rescanning already scanned parts, which makes it less practical in the field, especially in more complex forests. Potentially it might be solved by SLAM algorithm implementation.

Overall, TLS provided the most accurate and reliable results. Nevertheless, the performance of iPad Pro with the LiDAR sensor had the DBH estimation accuracy and tree detection rate closest to the TLS results when PLS_{hh} and MultiCam are considered for comparison.

Funding

This work was supported by grant No. CZ.02.1.01/0.0/0.0/16_019/0000803 (“Advanced research supporting the forestry and wood-processing sector’s adaptation to global change and the 4th industrial revolution”) financed by OP RDE, by the Scientific Grant Agency of the Ministry of Education, Science, Research, and Sport of the Slovak Republic and the Slovak Academy of Sciences [grant number VEGA 1/0335/20] and by the Internal Grant Agency of the Faculty of Forestry and Wood Technology, Mendel University in Brno, Czech Republic, grant number LDF_TP_2019012 “Remote Sensing to Support the Sustainability of Forest Production Under the Condition of Ongoing Climate Change”.

Declaration of Competing Interest

The authors declare that they have no known competing financial interests or personal relationships that could have appeared to influence the work reported in this paper.

Appendix A

Tables A1–A8.

Table A1
Tree detection rate (%) of all devices used for each plot are reported.

	A	B	C	D	E	F	G	H
TLS	100	90.6	93.5	95.8	93.5	100	95.2	93.5
PLS_{hh}	74.3	56.2	74.2	75	67.7	55.6	71.4	67.4
iPad	80	81.2	77.4	87.5	64.5	74.1	78.6	76.1
MultiCam	68.6	71.9	67.7	58.3	61.3	63	57.1	65.2

Table A2
Falsely detected trees (n) of all devices used for each plot are reported.

	A	B	C	D	E	F	G	H
TLS	2	3	2	3	1	0	1	0
PLS_{hh}	3	1	0	1	0	3	2	0
iPad	0	0	0	0	0	0	0	0
MultiCam	25	12	18	16	19	14	12	21

Table A3
BIAS (cm) of all devices used for each plot are reported.

	A	B	C	D	E	F	G	H
TLS	−0.92	−0.96	−0.95	−1.43	−1.14	−1.15	−0.86	−0.7
PLS_{hh}	5.55	4.59	3.5	2.82	2.58	4.85	3.97	6
iPad	−2.59	−2.6	−2.17	−1.79	−2.15	−1.8	−1.95	−1.87
MultiCam	−1.62	2.53	−1.33	−5.04	−1.65	−0.12	1.3	−1.78

Table A4
rBIAS (%) of all devices used for each plot are reported.

	A	B	C	D	E	F	G	H
TLS	3.67	3.37	3.19	4.32	3.85	3.67	3.44	2.67
PLS_{hh}	19.21	12.94	10.03	7.78	7.03	13.33	13.41	18.95
iPad	9.87	8.87	6.93	5.57	7.07	5.88	7.51	6.79
MultiCam	6.05	9.9	3.83	13.5	5.1	0.37	4.5	5.9

Table A5
RMSE (cm) of all devices used for each plot are reported.

	A	B	C	D	E	F	G	H
TLS	1.3	1.4	1.7	2	1.9	1.5	1.2	1
PLS_{hh}	6.3	8.8	5.2	4.8	5	5.3	5.6	7.5
iPad	3.4	3.4	3.3	3.3	2.9	2.6	3.2	2.8
MultiCam	5.1	5.9	4.9	14.3	8.6	7.1	4.3	5.4

Table A6
rRMSE (%) of all devices used for each plot are reported.

	A	B	C	D	E	F	G	H
TLS	5	4.9	5.6	6	6.4	4.7	4.7	3.7
PLS_{hh}	21.9	24.9	15	13.1	13.6	14.7	18.8	23.7
iPad	12.9	11.5	10.5	10.4	9.4	8.6	12.5	10.3
MultiCam	19.1	23	14	38.2	26.7	21.9	14.8	18.1

Table A7
Analysis of variance results.

	term	df	sumsq	meansq	statistic	p value
1	Device	3	0.470974	0.156991	99.34317	1.66E−54
2	Plot	7	0.024285	0.003469	2.195353	0.032723
3	Device:Plot	21	0.072798	0.003467	2.193635	0.001581
4	Residuals	784	1.238951	0.00158	NA	NA

Table A8
Absolute and relative root mean square error and tree detection rate for used devices across all eight plots for trees with DBH higher than 7 cm, 10 cm and 20 cm are reported.

	RMSE (cm)			rRMSE (%			TDR (%)		
	>7	>10	>20	>7	>10	>20	>7	>10	>20
TLS	1.45	1.51	1.67	5.18	4.86	4.33	95.15	96.07	100
PLS_{hh}	6.26	6.24	6.09	18.88	18.3	15.7	67.91	76.42	92.16
iPad	3.14	3.21	3.58	10.89	10.5	9.65	77.24	82.97	88.24
MultiCam	6.98	7.16	8.00	22.86	22.4	21.1	64.18	70.3	78.43

References

Balenović, I., Liang, X., Jurjević, L., Hyyppä, J., Seletković, A., Kukko, A., 2021. Hand-Held Personal Laser Scanning – Current Status and Perspectives for Forest Inventory Application. Croat. J. Eng. 19.

Bauwens, S., Bartholomeus, H., Calders, K., Lejeune, P., 2016. Forest Inventory with Terrestrial LiDAR: A Comparison of Static and Hand-Held Mobile Laser Scanning. Forests 7, 127. https://doi.org/10.3390/f7060127.

Boboc, R.G., Duguleană, M., Voinea, G.-D., Postelnicu, C.-C., Popovici, D.-M., Carrozzino, M., 2019. Mobile Augmented Reality for Cultural Heritage: Following the Footsteps of Ovid among Different Locations in Europe. Sustainability 11, 1167. https://doi.org/10.3390/su11041167.

Cabo, C., Del Pozo, S., Rodríguez-Gonzálvez, P., Ordóñez, C., González-Aguilera, D., 2018. Comparing Terrestrial Laser Scanning (TLS) and Wearable Laser Scanning (WLS) for Individual Tree Modeling at Plot Level. Remote Sens. 10, 540. https://doi.org/10.3390/rs10040540.

Čerňava, J., Mokroš, M., Tuček, J., Antal, M., Slatkovská, Z., 2019. Processing Chain for Estimation of Tree Diameter from GNSS-IMU-Based Mobile Laser Scanning Data. Remote Sens. 11, 615. https://doi.org/10.3390/rs11060615.

Chen, S., Liu, H., Feng, Z., Shen, C., Chen, P., 2019. Applicability of personal laser scanning in forestry inventory. PLoS ONE 14, e0211392. https://doi.org/10.1371/journal.pone.0211392.

Chudý, F., Slámová, M., Tomaštík, J., Tunák, D., Kardoš, M., Saloň, Š., 2018. The application of civic technologies in a field survey of landslides. Land Degrad. Dev. 29, 1858–1870. https://doi.org/10.1002/ldr.2957.

Del Perugia, B., Giannetti, F., Chirici, G., Travaglini, D., 2019. Influence of Scan Density on the Estimation of Single-Tree Attributes by Hand-Held Mobile Laser Scanning. Forests 10, 277. https://doi.org/10.3390/f10030277.

Durrant-Whyte, H., Bailey, T., 2006. Simultaneous localization and mapping: part I. IEEE Rob. Autom. Mag. 13, 99–110. https://doi.org/10.1109/MRA.2006.1638022.

Fabrika, M., Valent, P., Scheer, Ľ., 2018. Thinning trainer based on forest-growth model, virtual reality and computer-aided virtual environment. Environ. Model. Softw. 100, 11–23. https://doi.org/10.1016/j.envsoft.2017.11.015.

Fan, Y., Feng, Z., Mannan, A., Khan, T.U., Shen, C., Saeed, S., 2018. Estimating Tree Position, Diameter at Breast Height, and Tree Height in Real-Time Using a Mobile Phone with RGB-D SLAM. Remote Sens. 10, 1845. https://doi.org/10.3390/rs10111845.

Forsman, M., Börlin, N., Holmgren, J., 2016a. Estimation of Tree Stem Attributes Using Terrestrial Photogrammetry with a Camera Rig. Forests 7, 61. https://doi.org/10.3390/f7030061.

Forsman, M., Holmgren, J., Olofsson, K., 2016b. Tree Stem Diameter Estimation from Mobile Laser Scanning Using Line-Wise Intensity-Based Clustering. Forests 7, 206. https://doi.org/10.3390/f7090206.

Gollob, C., Ritter, T., Nothdurft, A., 2020. Forest Inventory with Long Range and High-Speed Personal Laser Scanning (PLS) and Simultaneous Localization and Mapping (SLAM) Technology. Remote Sens. 12, 1509. https://doi.org/10.3390/rs12091509.

Hyyppä, E., Yu, X., Kaartinen, H., Hakala, T., Kukko, A., Vastaranta, M., Hyyppä, J., 2020. Comparison of Backpack, Handheld, Under-Canopy UAV, and Above-Canopy UAV Laser Scanning for Field Reference Data Collection in Boreal Forests. Remote Sens. 12, 3327. https://doi.org/10.3390/rs12203327.

Hyyppä, J., Virtanen, J.-P., Jaakkola, A., Yu, X., Hyyppä, H., Liang, X., 2018. Feasibility of Google Tango and Kinect for Crowdsourcing Forestry Information. Forests 9, 6. https://doi.org/10.3390/f9010006.

Jurjević, L., Liang, X., Gašparović, M., Balenović, I., 2020. Is field-measured tree height as reliable as believed – Part II, A comparison study of tree height estimates from conventional field measurement and low-cost close-range remote sensing in a deciduous forest. ISPRS J. Photogramm. Remote Sens. 169, 227–241. https://doi.org/10.1016/j.isprsjprs.2020.09.014.

Kukko, A., Kaartinen, H., Hyyppä, J., Chen, Y., 2012. Multiplatform Mobile Laser Scanning: Usability and Performance. Sensors 12, 11712–11733. https://doi.org/10.3390/s120911712.

Liang, X., Hyyppä, J., Kaartinen, H., Lehtomäki, M., Pyörälä, J., Pfeifer, N., Holopainen, M., Brolly, G., Francesco, P., Hackenberg, J., Huang, H., Jo, H.-W., Katoh, M., Liu, L., Mokroš, M., Morel, J., Olofsson, K., Poveda-Lopez, J., Trochta, J., Wang, D., Wang, J., Xi, Z., Yang, B., Zheng, G., Kankare, V., Luoma, V., Yu, X., Chen, L., Vastaranta, M., Saarinen, N., Wang, Y., 2018a. International benchmarking of terrestrial laser scanning approaches for forest inventories. ISPRS J. Photogramm. Remote Sens. 144, 137–179. https://doi.org/10.1016/j.isprsjprs.2018.06.021.

Liang, X., Hyyppä, J., Kukko, A., Kaartinen, H., Jaakkola, A., Yu, X., 2014. The Use of a Mobile Laser Scanning System for Mapping Large Forest Plots. IEEE Geosci. Remote Sens. Lett. 11, 1504–1508. https://doi.org/10.1109/LGRS.2013.2297418.

Liang, X., Kankare, V., Hyyppä, J., Wang, Y., Kukko, A., Haggrén, H., Yu, X., Kaartinen, H., Jaakkola, A., Guan, F., Holopainen, M., Vastaranta, M., 2016. Terrestrial laser scanning in forest inventories. ISPRS J. Photogramm. Remote Sens. 115, 63–77. https://doi.org/10.1016/j.isprsjprs.2016.01.006.

Liang, X., Kukko, A., Hyyppä, J., Lehtomäki, M., Pyörälä, J., Yu, X., Kaartinen, H., Jaakkola, A., Wang, Y., 2018b. In-situ measurements from mobile platforms: An emerging approach to address the old challenges associated with forest inventories. ISPRS J. Photogramm. Remote Sens. 143, 97–107. https://doi.org/10.1016/j.isprsjprs.2018.04.019.

Liang, X., Wang, Y., Jaakkola, A., Kukko, A., Kaartinen, H., Hyyppä, J., Honkavaara, E., Liu, J., 2015. Forest Data Collection Using Terrestrial Image-Based Point Clouds From a Handheld Camera Compared to Terrestrial and Personal Laser Scanning. IEEE Trans. Geosci. Remote Sens. 53, 5117–5132. https://doi.org/10.1109/TGRS.2015.2417316.

McGlade, J., Wallace, L., Hally, B., White, A., Reinke, K., Jones, S., 2020. An early exploration of the use of the Microsoft Azure Kinect for estimation of urban tree Diameter at Breast Height. Remote Sens. Lett. 11, 963–972. https://doi.org/10.1080/2150704X.2020.1802528.

Mikita, T., Janata, P., Surový, P., 2016. Forest Stand Inventory Based on Combined Aerial and Terrestrial Close-Range Photogrammetry. Forests 7, 165. https://doi.org/10.3390/f7080165.

Mokroš, M., Liang, X., Surový, P., Valent, P., Čerňava, J., Chudý, F., Tunák, D., Saloň, Š., Merganič, J., 2018. Evaluation of Close-Range Photogrammetry Image Collection Methods for Estimating Tree Diameters. ISPRS Int. J. Geo-Inf. 7, 93. https://doi.org/10.3390/ijgi7030093.

Mokroš, M., Výbošťok, J., Grznárová, A., Bošela, M., Šebeň, V., Merganič, J., 2020. Non-destructive monitoring of annual trunk increments by terrestrial structure from motion photogrammetry. PLoS ONE 15, e0230082. https://doi.org/10.1371/journal.pone.0230082.

Piermattei, L., Karel, W., Wang, D., Wieser, M., Mokroš, M., Surový, P., Koreň, M., Tomaštík, J., Pfeifer, N., Hollaus, M., 2019. Terrestrial Structure from Motion Photogrammetry for Deriving Forest Inventory Data. Remote Sens. 11, 950. https://doi.org/10.3390/rs11080950.

Ryding, J., Williams, E., Smith, M.J., Eichhorn, M.P., 2015. Assessing Handheld Mobile Laser Scanners for Forest Surveys. Remote Sens. 7, 1095–1111. https://doi.org/10.3390/rs70101095.

Sarbolandi, H., Lefloch, D., Kolb, A., 2015. Kinect range sensing: Structured-light versus Time-of-Flight Kinect. Comput. Vis. Image Underst. 139, 1–20. https://doi.org/10.1016/j.cviu.2015.05.006.

Schöps, T., Sattler, T., Häne, C., Pollefeys, M., 2015. 3D Modeling on the Go: Interactive 3D Reconstruction of Large-Scale Scenes on Mobile Devices. In: 2015 International Conference on 3D Vision. Presented at the 2015 International Conference on 3D Vision, pp. 291–299. https://doi.org/10.1109/3DV.2015.40.

Tomaštík, J., Saloň, Š., Tunák, D., Chudý, F., Kardoš, M., 2017. Tango in forests – An initial experience of the use of the new Google technology in connection with forest inventory tasks. Comput. Electron. Agric. 141, 109–117. https://doi.org/10.1016/j.compag.2017.07.015.

Wang, Y., Lehtomäki, M., Liang, X., Pyörälä, J., Kukko, A., Jaakkola, A., Liu, J., Feng, Z., Chen, R., Hyyppä, J., 2019. Is field-measured tree height as reliable as believed – A comparison study of tree height estimates from field measurement, airborne laser scanning and terrestrial laser scanning in a boreal forest. ISPRS J. Photogramm. Remote Sens. 147, 132–145. https://doi.org/10.1016/j.isprsjprs.2018.11.008.

Wasenmüller, O., Stricker, D., 2017. Comparison of Kinect V1 and V2 Depth Images in Terms of Accuracy and Precision. In: Chen, C.-S., Lu, J., Ma, K.-K. (Eds.), Computer Vision – ACCV 2016 Workshops, Lecture Notes in Computer Science. Springer International Publishing, Cham, pp. 34–45. https://doi.org/10.1007/978-3-319-54427-4_3.